JACS
JOURNAL OF THE AMERICAN CHEMICAL SOCIETY
Article
pubs.acs.org/JACS

Toward Fundamentals of Confined Catalysis in Carbon Nanotubes

Jianping Xiao, Xiulian Pan,* Shujing Guo,† Pengju Ren, and Xinhe Bao*

State Key Laboratory of Catalysis, Dalian Institute of Chemical Physics, Chinese Academy of Science, Zhongshan Road 457, Dalian 116023, P. R. China

Supporting Information

ABSTRACT: An increasing number of experimental studies have demonstrated that metal or metal oxide nanoparticles confined inside carbon nanotubes (CNTs) exhibit different catalytic activities with respect to the same metals deposited on the CNT exterior walls, with some reactions enhanced and others hindered. In this article, we describe the concept of confinement energy, which enables prediction of confinement effects on catalytic activities in different reactions. Combining density functional theory calculations and experiments by taking typical transition metals such as Fe, FeCo, RhMn, and Ru as models, we observed stronger strains and deformations within the CNT channels due to different electronic structures and spatial confinement. This leads to downshifted d-band states, and consequently the adsorption of molecules such as CO, N_2, and O_2 is weakened. Thus, the confined space of CNTs provides essentially a unique microenvironment due to the electronic effects, which shifts the volcano curve of the catalytic activities toward the metals with higher binding energies. The extent of the shift depends on the specific metals and the CNT diameters. This concept generalizes the diverse effects observed in experiments for different reactions, and it is anticipated to be applicable to an even broader range of reactions other than redox of metal species, CO hydrogenation, ammonia synthesis and decomposition discussed here.

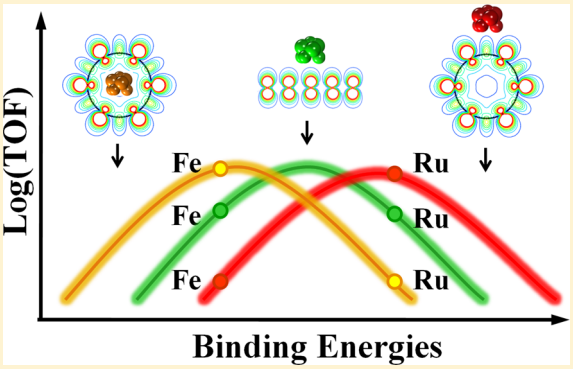

INTRODUCTION

Well-defined nanocavities of zeolites and mesoporous silica are recognized to open up the prospect of performing heterogeneous catalysis in a novel manner.[1,2] Some of the reaction pathways might be hindered or even blocked due to the spatial restriction and the interactions at the interfaces.[3] Thus, the activity and/or product selectivity are modulated, as observed in chiral hydrogenation, oxidation, and amination.[3,4] Carbon nanotubes (CNTs) are a new type of porous materials, characterized with nearly one-dimensional nanocavities formed by the curved graphene walls. Recently, an increasing number of experimental studies demonstrated that within these nanocavities metal or metal oxide nanoparticles exhibit different catalytic activities with respect to the same metals deposited on the CNT exterior walls.[5,6] For instance, the reduction of Fe_2O_3 nanoparticles (NPs) supported on the CNTs exteriors required a temperature higher than 1070 K, while those encapsulated in the CNT channels with an inner diameter of ∼8 nm could be reduced at a much lower temperature (∼900 K). The reduction became more facile and the temperature lowered to ∼860 K when the inner diameter of CNTs was reduced to ∼2 nm.[7,8] In contrast, the oxidation of encapsulated metallic Fe NPs was retarded in comparison to that of the outside particles.

Over such encapsulated Fe NPs, Fischer−Tropsch synthesis (FTS) was enhanced with respect to the outside Fe particles, although the latter were more accessible to reactants.[9] CO conversion was almost 1.5 times, and the yield in C_{5+} hydrocarbons was twice as high as that on the outside catalyst.[9] Similarly, a bicomponent RhMn catalyst was also found to benefit from being confined within the CNT channels in syngas conversion to C_2 oxygenates.[10] Zhang et al. reported that an FeCo alloy encapsulated in CNTs with an inner diameter as large as ∼40 nm facilitated NH_3 decomposition[11] and gave a much superior stability. Serp and co-workers observed that the encapsulation of PtRu nanoparticles within CNTs enhanced significantly the selective hydrogenation of cinnamaldehyde.[12] The CNT-confined PtRu particles exhibited a turnover frequency (TOF) almost 3 times higher, and the selectivity toward cinnamyl alcohol (resulting from C═O bond hydrogenation) was linearly correlated to the percentage of the NPs located inside CNTs.[12] More recently, Centi and Perathoner found that gas-phase photoelectrocatalytic conversion of CO_2 to isopropanol and other alcohols/hydrocarbons was also promoted via encapsulation of Fe catalysts, and the product distribution was modulated as well.[13] However, encapsulation also exerts negative effects on some reactions. For example, the CNT-confined Ru nanoparticles exhibited a lower activity in ammonia synthesis than the outside catalyst, even though exactly the same batch of CNTs had been used and the two catalysts kept a similar Ru particle size before and after reactions.[14] A similar negative effect was also reported for Ru

Received: November 8, 2014
Published: December 14, 2014

DOI: 10.1021/ja511498s
J. Am. Chem. Soc. 2015, 137, 477−482

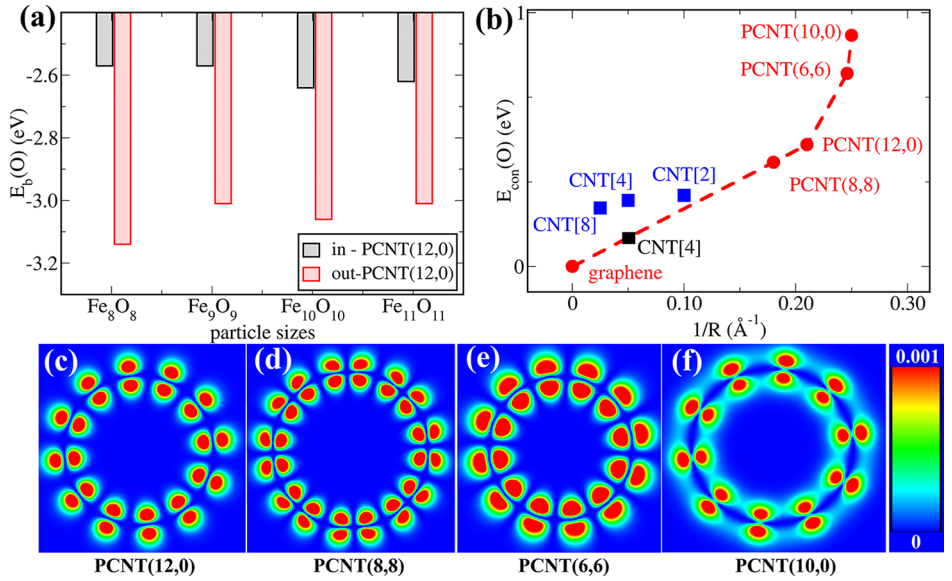

Figure 1. (a) Oxygen binding energies, E_b(O), of Fe_nO_n (n = 8−11) clusters encapsulated within PCNT(12, 0) (in-PCNT) in comparison to the clusters sitting on its exterior wall (out-PCNT). (b) Confinement energy, E_{con}(O), for Fe_9O_9 clusters within PCNTs as a function of the CNT diameters, with the blue and black squares representing E_{con} estimated from the reduction of iron oxide and oxidation of metallic iron nanoparticles within CNTs with the inner diameter of about 8, 4, and 2 nm,[7] following eqs 3 and 4. (c−f) The electronic polarization and distribution at the valence band maximum of (c) PCNT(12, 0), (d) PCNT(8, 8), (e) PCNT(6, 6), and (f) PCNT(10, 0) (unit = e/a.u.^{2}).

catalyst in ammonia decomposition.[15] These studies demonstrate that the confined space of CNTs does allow fine-tuning of catalytic performance without changing the catalyst composition, although the confinement effects may vary with reactions and metals. Therefore, we herein look into the underlying mechanism for these diverse effects, which is crucial for rational design of efficient catalysts.

The structures of the CNT encapsulates were analyzed taking typical transition metal catalysts Fe, Ru, and bicomponent FeCo and RhMn as models, in comparison to the outside clusters, i.e., clusters located on the CNT exterior walls. By combining density functional theory (DFT) calculations and experiments, we show that the above diverse effects can be well described by the concept of "confinement energy (E_{con})", which allows prediction of the catalytic activities in, e.g., redox of metal species, CO hydrogenation, ammonia synthesis and decomposition.

THEORETICAL ATOMISTIC MODELS

We set out with simple reactions, i.e., oxidation of iron by oxygen and reduction of iron oxides. This can be characterized by the binding energies of oxygen E_b(O):

$$E_b(\mathrm{O}) = \left[E(\mathrm{MO}_n) - E(\mathrm{M}) - n\frac{1}{2}\mu(\mathrm{O}_2)\right]/n \quad (1)$$

where $E(\mathrm{MO}_n)$ and E(M) represent the total energies of the CNT-encapsulated or CNT-supported metal oxide and metal clusters, respectively. $\mu(\mathrm{O}_2)$ is the chemical potential of a free O_2 molecule. Fe_9 and Fe_9O_n clusters were taken as models, with n = 1−9 reflecting different extents of oxidation. For simplicity of calculations, we took CNTs with two representative chiralities, i.e., armchair CNT (8, 8) and zigzag CNT (12, 0), with a diameter of ∼1.0 nm as models. Since chemically synthesized CNTs are frequently concomitant with defects, CNTs (8, 8) and (12, 0) with a single carbon vacancy were used to model defected tubes (denoted as DCNT) with respect to perfect ones (PCNT). The effects of the semiconducting and metallic properties are also considered by comparing CNTs (10, 0) and (6, 6), which have a comparable diameter.

The microkinetic model analysis was carried out for understanding the confinement effects on reactions such as Fischer−Tropsch synthesis (FTS), ammonia synthesis and decomposition in comparison to the experimental results. The CNT-encapsulated and CNT-supported metal clusters were abbreviated as M-*in* and M-*out* (M = Fe, FeCo, RhMn, and Ru), respectively. More computational details are given in the Supporting Information.

RESULTS AND DISCUSSION

Taking PCNT(12, 0) for an example, the averaged E_b(O) on Fe-*out* is −3.35 eV/O, which is much smaller than that on a free-standing Fe_9 cluster (−4.59 eV/O). As listed in Supporting Information, Table S1, when the Fe_9 cluster is moved into the confined space of the CNT, the averaged E_b(O) lowers to −3.06 eV/O, suggesting that the oxygen binding is weaker over the encapsulated Fe_9 cluster than that over the outside Fe_9 cluster. E_b(O) decreases at a higher oxygen coverage, and it lowers by ∼0.5 eV/O compared to the exterior binding at a 1 ML coverage (Fe_9O_9) (Figure 1a). A similar trend is observed for a defected CNT, i.e., weakened E_b(O) over a DCNT-encapsulated Fe_9 cluster (see the Supporting Information for more details). Figure 1a shows that the difference of E_b(O) between Fe-*in* and Fe-*out* for Fe_8O_8, Fe_9O_9, $Fe_{10}O_{10}$, and $Fe_{11}O_{11}$, which have a size of 4−6 Å, falls in a range of 0.3−0.5 eV/O.

In order to understand the underlying mechanism, we analyzed the electronic structures of the encapsulates. As shown in Supporting Information, Figure S1, the d-band states of the encapsulated Fe_9 clusters are shifted downward due to the stronger interactions of the encapsulated Fe clusters with the interior surface of CNTs, reflected by the stronger strains and deformation within the confined nanospace. This is also affected by the different electronic structures and polarization at the Fermi levels of CNTs, as demonstrated by CNTs with different chiralities and diameters in Figure 1c−f. As the effective d-band states centers affect the occupancy of antibonding states of the adsorbed O atoms,[16] a lower d-

DOI: 10.1021/ja511498s
J. Am. Chem. Soc. 2015, 137, 477−482

band center would lead to more occupancy. This results in a weaker binding of O atoms. It is known that the E_b(O) can be sensitive to the structures of clusters.[17] Therefore, we took Fe(110) surfaces with different strains as models for comparison, which exclude the effects of structure sensitivity. The results in Supporting Information, Figure S2, show that strained surfaces also lead to downshifted d-band states and weakened binding energies, consistent with the confined catalysts. It reveals again the importance of the electronic structure. The weakened E_b(O) implies that the encapsulated Fe clusters are more difficult to oxidize than those located on the exterior walls of CNTs. The weaker oxygen binding energy, the more difficult to oxidize. This trend is consistent with our experimental observation for the retarded oxidation of the encapsulated metallic Fe within CNTs.[7]

Since E_b(O) differs between the CNT-encapsulated and CNT-supported Fe_9 only because of different locations of the clusters, i.e., on the exterior or interior walls of CNTs, we define their differences as the confinement energy E_{con}:

$$E_{con} = E_b(\text{in}) - E_b(\text{out}) \quad (2)$$

where E_b(in) and E_b(out) are the binding energies of molecules over an encapsulated metallic cluster and a cluster sitting on the exterior wall of the same CNT, respectively. Note that E_{con} is different from the energy of encapsulating an atom or molecule into the nanotube. Figure 1b shows that E_{con}(O) is sensitive to the diameter of CNTs. It is zero for a planar graphene and increases with the decreasing CNT diameter. There is a dramatic increase for nanotubes smaller than 1.0 nm. For example, E_{con}(O) ≈ 0.45 eV for a PCNT(8, 8), and it jumps to ~0.9 eV for a PCNT(10, 0). It implies that the inside and outside difference in E_b(O) becomes larger, i.e., a stronger confinement effect within smaller nanotubes. This is understandable considering that the sp^2 hybridization is deformed much more with the increasing curvature. The higher E_{con}(O) suggests that it is more difficult to oxidize the encapsulated iron cluster and more facile to reduce iron oxide. This is consistent with our previous experimental observation that the encapsulated Fe_2O_3 NPs within smaller diameter CNTs are reduced at a lower temperature.[7] Although the simulated CNTs here are smaller than the previously experimentally studied ones (inner diameters = 2−8 nm), the essential effects of confinement within different sized CNTs on the E_b(O) can already be captured by these simple CNT models. This is further confirmed by estimation of E_{con}(O) for the larger nanotubes CNT[4] (with the number in square bracket denoting the inner diameter) from the oxidation temperature of encapsulated iron,[7] following eqs 3 and 4. It gives E_{con}(O) ≈ 0.11 eV, represented by the black square in Figure 1b. Furthermore, E_{con}(O) can also be estimated from experimental reduction of encapsulated iron oxide with CNT[8], CNT[4], and CNT[2].[7] This leads to blue squares, sitting slightly above the predicted curve in Figure 1b, likely due to a higher oxygen coverage. One sees obviously the monotonic decreasing trend of the confinement energy as a function of the CNT diameter.

Furthermore, Figure 1b shows that E_{con}(O) for Fe@PCNT(10,0) is higher than that for Fe@PCNT(6,6), although both have a comparable diameter. This implies that the semiconducting tube provides a stronger confinement effect, protecting Fe clusters from oxidation with respect to the metallic PCNT(6,6). This is likely attributed to their different electronic structures. The semiconducting PCNT(10,0) has more delocalized electron at the cross section of the CNT and higher aromaticity,[18] which makes oxygen binding even weaker on the encapsulated iron. Further examination on E_{con}(O) of the Re_9 clusters reveals a similar trend, as E_{con}(O) = 0.65 eV for Re@CNT(6,6) and E_{con}(O) = 1.30 eV for Re@CNT(10,0). Thus, Re clusters encapsulated within the semiconducting CNT will be more difficult to oxidize than in metallic one, agreeing well with our previous experimental findings.[19] This demonstrates the important role of the electronic structures in addition to the spatial restriction playing in the confinement effects.

The above results show that E_{con}(O) reflects the confinement strength on the redox reactions of metal species. From E_{con}(O), we can estimate the temperature difference required to reduce the inside and outside metal oxide clusters following *ab initio* thermodynamics analysis,[20] as shown in eqs 3 and 4:

$$\frac{1}{2}\mu(O_2) = \frac{1}{2}E(O_2) + \Delta\mu_O \quad (3)$$

$$\Delta\mu_O = \Delta H(T) - \Delta S(T)\Delta T \quad (4)$$

where $\mu(O_2)$ is the chemical potential of O_2, calculated from the energy of an isolated O_2 molecule, $E(O_2)$ and $\Delta\mu_O$. $\Delta H(T)$ and $\Delta S(T)$ refer to the experimentally measured enthalpy change and entropy change under the standard pressure.[21] At the thermodynamic equilibrium, the critical E_b(O) can be assumed to be 0 eV when a Fe_9O_9 cluster is fully reduced to metallic Fe_9. Therefore, one can estimate the temperature difference (ΔT) to be about 300 K for PCNT(8,8); i.e., the encapsulated Fe_9O_9 cluster can be reduced at a temperature 300 K lower than the outside cluster, as displayed in Figure 2.

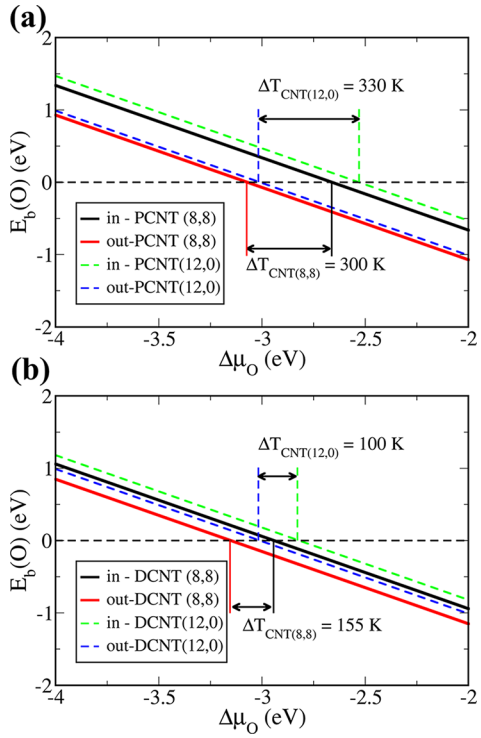

Figure 2. Oxygen binding energies, E_b(O), over the encapsulated Fe_9O_9 with respect to the outside Fe_9O_9 cluster as a function of the chemical potential change of oxygen ($\Delta\mu_O$), where $\mu(O_2) = E(O_2) + 2\Delta\mu_O$, and $E(O_2)$ refers to an isolated O_2. (a) PCNTs and (b) DCNTs. The chemical potential change of oxygen, $\Delta\mu_O$, was obtained from the thermodynamics database.[20]

DOI: 10.1021/ja511498s
J. Am. Chem. Soc. 2015, 137, 477−482

Within a smaller nanotube such as CNT(12, 0), the reduction temperature for the encapsulated Fe_9O_9 is lowered by 330 K compared to the outside one, suggesting a more facile reduction. For DCNTs, we observed a similar trend but with smaller temperature difference. ΔT is ~155 K for DCNT(8, 8) and ~100 K for DCNT(12, 0), respectively. This indicates that the confinement effect is weaker in DCNTs than that in PCNTs. In comparison, the experimentally observed ΔT was ~200 K for the reduction of Fe_2O_3 NPs within CNTs with an inner diameter of 4−8 nm, and the ΔT was ~85 K for the oxidation of Fe within the same CNTs.[7] Considering the diameter and oxygen coverage dependence of the confinement strength (Figure 1b), and the presence of defects on experimental CNTs, the theoretically predicted ΔT here is consistent qualitatively with the experimental values. The above discussions reveal that the confinement effects and the modification extent on the redox properties of encapsulated metals can be well described by the confinement energy, originating from weakened oxygen binding.

It is interesting to note that the dissociative binding energies of other molecules such as CO and N_2, E_b(CO) and $E_b(N_2)$, also follow a similar trend as E_b(O), i.e., weaker over the encapsulated Fe_9 cluster than that over the outside one (Figure 3). More interestingly, the same trend is observed for other

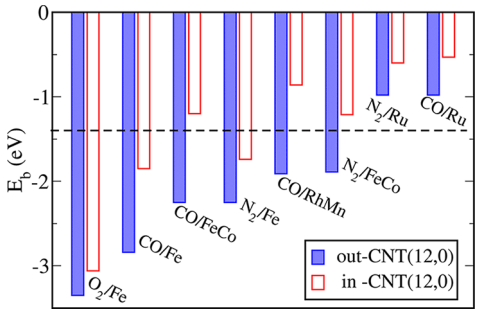

Figure 3. Dissociative binding energies of CO, N_2, and O_2 molecules on typical transition metal clusters (Fe, FeCo, RhMn, and Ru) encapsulated within PCNT (12, 0) in comparison to those located on the exterior walls, denoted as in-CNT(12, 0) and out-CNT(12, 0), respectively. The optimal E_b(CO) and $E_b(N_2)$ for CO hydrogenation and ammonia synthesis, obtained from microkinetic model, is indicated by the dashed line for comparison.

transition metals such as Ru, and even bicomponent RhMn and FeCo, which have been studied experimentally in CO, N_2 hydrogenation, and NH_3 decomposition. It implies that the weakened binding of molecules over the encapsulated metal clusters is likely a general feature, although the molecules and metals possess very different intrinsic properties. However, the confinement energies, E_{con}(CO) and $E_{con}(N_2)$, vary with the individual metals within the same type of CNTs, suggesting the confinement effects are metal-specific, as $E_{con}(O_2)$. Therefore, this can be explored for prediction of catalytic activities since the (dissociative) adsorption of molecules is frequently the rate-determining step in catalytic reactions.

Taking CO hydrogenation for an example, the dissociation of CO is generally considered as the rate-determining step.[22] Thus, the overall reaction rate, r, can be written as

$$r = 2kP(\mathrm{CO})\theta^{*2} \quad (5)$$

where k is the rate constant for CO dissociation in the forward direction, P(CO) is the partial pressure of CO gas, and θ^* is the surface coverage of free active sites. The overall reaction was assumed reaching the equilibrium.

In the light of Sabatier principle[23] and the Brønsted−Evans−Polanyi (BEP) relation,[24] the catalytic activity can be correlated with the dissociative binding energies of the reactant on the catalyst surface with a volcano curve. The activity increases with the dissociative binding energy and reaches a maximum, and then it drops if the binding is too strong. Therefore, catalytic reactions require an intermediate binding strength of the reactant in order to achieve an optimal activity. According to the microkinetic model analysis, the TOF of CO hydrogenation can be plotted as a function of the dissociative binding energy of CO, E_b(out), on the supported metal catalysts, as the black curve in Figure 4a. The optimal E_b(CO) is around −1.44 eV for

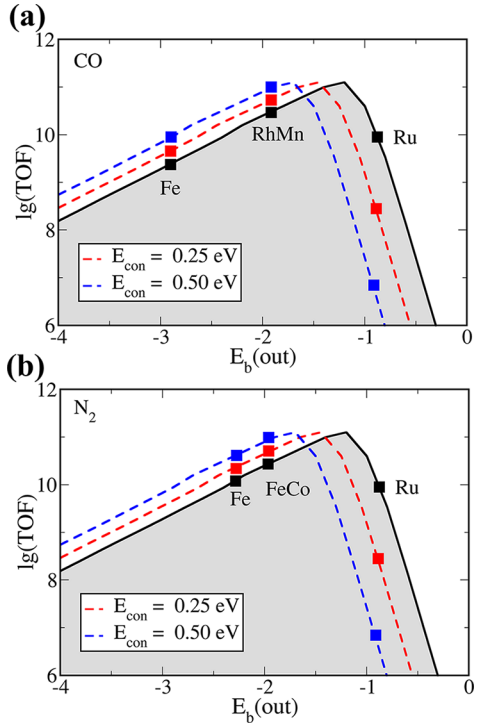

Figure 4. Calculated turnover frequencies (TOF) as a function of the dissociative binding energy E_b(out) of (a) CO and (b) N_2 on a variety of catalysts (M = Fe, FeCo, RhMn, and Ru). The black curves correspond to the catalysts supported on the exterior walls of CNTs, and the red and blue curves represent the encapsulated catalysts at E_{con} = 0.25 and 0.50 eV, respectively, where E_b(in) = E_b(out) + E_{con}. $P(N_2)$ and P(CO) are set to 3 MPa, and T = 600 K in the microkinetic models.

CO conversion. However, E_b(CO) is −2.84 eV/CO over the Fe-*out* catalyst, sitting on the left-hand side of the volcano curve. The binding is too strong, making it difficult for further hydrogenation. In comparison, E_b(CO) is reduced by ~1.0 eV/CO over Fe-*in*, which makes the dissociatively adsorbed CO species easier to react with hydrogen, hence leaving more active sites (θ^*) free for further CO adsorption. Thus, the activity of Fe-*in* is predicted to be higher than Fe-*out*, as marked by the red square in Figure 4, according to eq 5 and E_b(in) = E_b(out) + E_{con}. This is in agreement with the previous experimental observation of enhanced FTS reaction over the encapsulated Fe catalyst with respect to the same metal NPs locating on the CNT exterior walls although the latter are much more accessible to reactants.[9] Figure 4 demonstrates that a stronger

DOI: 10.1021/ja511498s
J. Am. Chem. Soc. 2015, 137, 477−482

confinement strength would promote further the reaction. For example, TOF can rise from about $10^{9.5}$ to 10^{10} when E_{con} increases from 0.25 (the red curve) to 0.50 eV (the blue curve). Similarly, an enhanced syngas conversion can also be predicted for the encapsulated RhMn, as we observed experimentally.[10]

In comparison, E_b(CO) over Ru-*out* is smaller than −1.44 eV, located on the right-hand side of the volcano curve. E_b(CO) is even lower over Ru-*in*. Therefore, a lower TOF can be predicted for Ru-*in* with respect to Ru-*out* (Figure 4), i.e., a negative effect from confinement on Ru catalyzed CO conversion. A stronger confinement effect would suppress further the activity of Ru catalysts, as demonstrated. This effect is opposite to the one observed for CO hydrogenation over Fe and RhMn catalysts.[9,10] The prediction is consistent with the experimental results of FTS over Ru-*in* and Ru-*out*, as shown in the Supporting Information, Figure S3. Careful efforts have been made to prepare Ru-*in* and Ru-*out* with a similar particle size distribution and similar Ru loadings. The microcalorimetry of CO adsorption showed that the initial differential heat of CO adsorption over Ru-*in* was 12 kJ/mol lower than that over Ru-*out*,[14] indicating a weaker adsorption on the encapsulated Ru catalyst. The CO conversion rate over Ru-*in* turns out to be lower than that over Ru-*out*. Following the same theory and the data in Figures 3 and 4, a lower ammonia synthesis activity, i.e., hydrogenation of N_2, can be predicted for the encapsulated Ru as well, since the dissociative binding energy of N_2 is lower over Ru-*in* than that over Ru-*out* and both are lower than −1.44 eV, located on the right-hand side of the volcano curve. The negative effect of confinement on Ru catalyzed ammonia synthesis has been experimentally observed previously.[14] Therefore, the confinement essentially provides a micro-environment, which shifts the volcano curve toward the metals with a higher binding energy. The extent of the shift depends on the confinement energy. To further check the validity of the concept of confinement energy, we analyzed ammonia decomposition in comparison to the experimentally reported results over FeCo and Ru catalysts.[11,15] Since it is the reverse reaction of ammonia synthesis, the TOF of NH_3 decomposition can be correlated with that of NH_3 synthesis by a factor of reversibility, γ, ($TOF_{de} = TOF_{syn}\gamma$),[25] which can be assumed comparable for the inside and outside catalysts. Thus, NH_3 decomposition can be analyzed using $E_b(N_2)$. Figure 3 shows that $E_b(N_2)$ is −2.25 eV/N_2 over FeCo-*out* while the N_2 binding becomes weaker within the CNT channels with $E_b(N_2)$ = −1.74 eV/N_2. As a result, the reaction should be facilitated over FeCo-*in* (Figure 4).[11] In contrast, a much lower ammonia decomposition activity is predicted for Ru-*in* than Ru-*out*, which is consistent with the experimental reports.[15] Therefore, we conclude that confinement within CNTs is a general feature, which provides a new approach to tune the catalytic activities. It can be anticipated that the concept of confinement energy can be used to predict the effects of confinement on reactions other than discussed here.

CONCLUSIONS

DFT calculations taking a variety of transition metal clusters, such as Fe, Re, Ru, FeCo, RhMn, reveal that confinement is an intrinsic property of CNTs, because of the nanospace formed by the curved graphene wall and the concomitant electronic structures. The d-band states of encapsulated metal clusters are downshifted with respect to the metal clusters sitting on the CNT exterior walls, leading to weakened binding of molecules over the encapsulated metal clusters due to the electronic effects. Thus, the unique confined environment essentially shifts the volcano curve of the catalytic activities toward the metals with higher binding energies, which can be well described by the confinement energy. With this concept, catalytic activities of these metal catalysts in reactions such as redox of metal species, CO hydrogenation, ammonia synthesis and decomposition are well predicted. Therefore, we anticipate that this concept can be further explored for rational design of efficient catalysts for a much wider range of reactions based on CNTs and even other porous materials with well-defined pore structures, such as mesoporous silica[26] and metal−organic frameworks.[27−29]

ASSOCIATED CONTENT

Supporting Information

E_b(O) at different coverage of oxygen over the Fe-*in* and Fe-*out* and a part of optimized geometries, experimentally measured activity of Ru-*in* and Ru-*out* in FTS synthesis, and the corresponding particle size distributions. This material is available free of charge via the Internet at http://pubs.acs.org.

AUTHOR INFORMATION

Corresponding Authors

panxl@dicp.ac.cn
xhbao@dicp.ac.cn

Present Address

†S.G.: Shaanxi Yanchang Petroleum (Group) Co., Ltd., 710075 Xi'an, Shaanxi, P.R. China.

Notes

The authors declare no competing financial interest.

ACKNOWLEDGMENTS

J.X. acknowledges financial support from China Postdoctoral Science Foundation (2014M551131) and Outstanding Postdoctoral Award (DMTO Project) from Dalian Institute of Chemical Physics, Chinese Academy of Science. The authors thank the Shanghai Supercomputer Center for computational resources. X.P. and X.B. acknowledge financial support from the Natural Science Foundation of China (21173215 and 21033009) and the Ministry of Science and Technology (2011CBA00503 and 2013CB933100).

REFERENCES

(1) Derouane, E. G. *J. Catal.* **1986**, *100*, 541.
(2) Serp, P.; Castillejos, E. *ChemCatChem* **2010**, *2*, 41.
(3) Thomas, J. M.; Raja, R. *Acc. Chem. Res.* **2008**, *41*, 708.
(4) Fraile, J. M.; García, J. I.; Herrerías, C. I.; Mayoral, J. A.; Pires, E. *Chem. Soc. Rev.* **2009**, *38*, 695.
(5) Pan, X.; Bao, X. *Chem. Commun.* **2008**, *47*, 6271.
(6) Pan, X.; Bao, X. *Acc. Chem. Res.* **2011**, *44*, 553.
(7) Chen, W.; Pan, X.; Bao, X. *J. Am. Chem. Soc.* **2007**, *129*, 7421.
(8) Chen, W.; Pan, X.; Willinger, M.-G.; Su, D. S.; Bao, X. *J. Am. Chem. Soc.* **2008**, *128*, 3136.
(9) Chen, W.; Fan, Z.; Pan, X.; Bao, X. *J. Am. Chem. Soc.* **2008**, *130*, 9414.
(10) Pan, X.; Fan, Z.; Chen, W.; Ding, Y.; Luo, H.; Bao, B. *Nat. Mater.* **2007**, *6*, 507.
(11) Zhang, J.; Müller, J.-O.; Zheng, W.; Wang, D.; Su, D. S.; Schlögl, R. *Nano Lett.* **2008**, *8*, 2738.
(12) Castillejos, E.; Debouttire, P.-J.; Roiban, L.; Solhy, A.; Martinez, V.; Kihn, Y.; Ersen, O.; Philippot, K.; Chaudret, B.; Serp, P. *Angew. Chem., Int. Ed.* **2009**, *48*, 2529.
(13) Centi, G.; Perathoner, S. *Catal. Today* **2010**, *150*, 151.

DOI: 10.1021/ja511498s
J. Am. Chem. Soc. 2015, 137, 477−482

(14) Guo, S.; Pan, X.; Gao, H.; Yang, Z.; Zhao, J.; Bao, X. *Chem.—Eur. J.* **2010**, *16*, 5379.
(15) Zheng, W.; Zhang, J.; Zhu, B.; Blume, R.; Zhang, Y.; Schlichte, K.; Schlögl, R.; Schueth, F.; Su, D. S. *ChemSusChem* **2009**, *3*, 226.
(16) (a) Hammer, B.; Nørskov, J. K. *Science* **2002**, *376*, 238. (b) Mavrikakis, M.; Hammer, B.; Nørskov, J. K. *Phys. Rev. Lett.* **1998**, *81*, 2819. (c) Xu, Y.; Ruban, A. V.; Mavrikakis, M. *J. Am. Chem. Soc.* **2004**, *126*, 4717. (d) Xiao, J.; Frauenheim, T. *J. Phys. Chem. C* **2013**, *117*, 1804. (e) Xiao, J.; Kuc, A.; Frauenheim, T.; Heine, T. *J. Mater, Chem. A* **2014**, *2*, 4885.
(17) Kim, G.; Kawazoe, Y.; Lee, K.-R. *J. Phys. Chem. Lett.* **2012**, *3*, 1989.
(18) Ren, P.; Zheng, A.; Xiao, J.; Pan, X.; Bao, X. *Chem. Sci.* **2014**, DOI: 10.1039/C4SC01996B.
(19) Zhang, F.; Pan, X.; Hu, Y.; Yu, L.; Chen, X.; Jiang, P.; Zhang, H.; Deng, S.; Zhang, J.; Bolin, T. B.; Zhang, S.; Huang, Y.; Bao, X. *Proc. Natl. Acad. Sci. U.S.A.* **2013**, *110*, 14861.
(20) (a) Stampfl, C.; Scheffler, M. *Phys. Rev. Lett.* **1997**, *78*, 1500. (b) Reuter, K.; Scheffler, M. *Phys. Rev. Lett.* **2003**, *90*, 046103. (c) Reuter, K.; Frenkel, D.; Scheffler, M. *Phys. Rev. Lett.* **2004**, *93*, 116105. (d) Li, W.-X.; Stampfl, C.; Scheffler, M. *Phys. Rev. Lett.* **2003**, *90*, 256102. (e) Xiao, J.; Frauenheim, T. *J. Phys. Chem. Lett.* **2012**, *3*, 2638. (f) Xiao, J.; Rosa, A. L.; Zhang, R.; Teoh, W. Y.; Frauenheim, T. *ChemCatChem* **2014**, *6*, 2322.
(21) Chase, M. W., Jr. *NIST-JANAF Themochemical Tables*, 4th ed., Journal of Physical and Chemical Reference Data Monograph *9*; NIST: Gaithersburg, MD, 1998; p 1.
(22) (a) Bligaard, T.; Nørskov, J. K.; Dahl, S.; Matthiesen, J.; Christensen, C. H.; Sehested, J. *J. Catal.* **2004**, *224*, 206. (b) Liu, J.-X.; Su, H.-Y.; Sun, D.-P.; Zhang, B.-Y.; Li, W.-X. *J. Am. Chem. Soc.* **2013**, *135*, 16284.
(23) Sabatier, P. *Ber. Dtsch. Chem. Ges.* **1911**, *44*, 1984.
(24) (a) Nørskov, J. K.; Bligaard, T.; Hvolbæk, B.; Abild-Pedersen, F.; Chorkendorff, I.; Christensen, C. H. *Chem. Soc. Rev.* **2008**, *37*, 2163. (b) Michaelides, A.; Liu, Z.-P.; Zhang, C. J.; Alavi, A.; King, D. A.; Hu, P. *J. Am. Chem. Soc.* **2003**, *125*, 3704. (c) Munter, T. R.; Bligaard, T.; Christensen, C. H.; Nørskov, J. K. *Phys. Chem. Chem. Phys.* **2008**, *10*, 5202. (d) Cheng, J.; Hu, P.; Ellis, P.; French, S.; Kelly, G.; Lok, C. M. *J. Phys. Chem. C* **2008**, *112*, 1308.
(25) Boisen, A.; Dahl, S.; Nørskov, J. K.; Christensen, C. H. *J. Catal.* **2005**, *230*, 309.
(26) Xiong, H.; Zhang, Y.; Wang, S.; Liew, K.; Li, J. *J. Phys. Chem. C* **2008**, *112*, 9706.
(27) Aijaz, A.; Xu, Q. *J. Phys. Chem. Lett.* **2014**, *5*, 1400.
(28) Aijaz, A.; Karkamkar, A.; Choi, Y. J.; Tsumori, N.; Rönnebro, E.; Autrey, T.; Shioyama, H.; Xu, Q. *J. Am. Chem. Soc.* **2012**, *134*, 13926.
(29) Jiang, H. L.; Liu, B.; Akita, T.; Haruta, M.; Sakurai, H.; Xu, Q. *J. Am. Chem. Soc.* **2009**, *131*, 11302.

DOI: 10.1021/ja511498s
J. Am. Chem. Soc. 2015, 137, 477−482